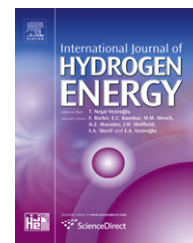


Available online at www.sciencedirect.com

SciVerse ScienceDirect

journal homepage: www.elsevier.com/locate/he

Visible light driven photocatalytic hydrogen evolution and photophysical properties of Bi³⁺ doped NaTaO₃

Pushkar Kanhere^a, Jianwei Zheng^b, Zhong Chen^{a,*}

^a School of Materials Science and Engineering, Nanyang Technological University, Block N4.1, 50 Nanyang Avenue, Singapore 639798, Singapore

^b Institute of High Performance Computing, 1 Fusionopolis Way, #16-16 Connexis, Singapore 138632, Singapore

ARTICLE INFO

Article history:

Received 19 September 2011

Received in revised form

7 December 2011

Accepted 10 December 2011

Available online 2 January 2012

Keywords:

NaTaO₃

Photocatalyst

Photocatalytic hydrogen

Band gap

Bismuth doping

Flat band potential

ABSTRACT

Visible light active Bismuth doped NaTaO₃ powders were synthesized by the conventional solid state route for different Bi concentrations (2.5%, 5.0%, and 7.5% by moles). The optical properties of the doped samples were tuned by changing the molar ratio of Na and Ta in the initial reactants. The doped samples prepared with Na/Ta ratio close to unity (1.01–1.03) resulted in the highest band gap narrowing compared to the other synthesis conditions. It was shown that the photocatalytic hydrogen evolution occurred from these samples under the visible light irradiation ($\lambda > 390$ nm) after loading of appropriate amount of platinum co-catalyst. The other synthesis conditions (Na/Ta = 1/1-x; x = 0.025, 0.05, 0.075 and Ta/Na = 1/1-x; x = 0.025, 0.05, 0.075; x is bismuth content) were not useful for the photocatalytic hydrogen evolution. The structural characterization suggested that the samples prepared with Na/Ta ratio close to unity, contain Bi ions located at both Na and Ta sites in the lattice. The Mott–Schottky plots revealed that the flat band potential of the pristine NaTaO₃ is highly negative to the H₂/H₂O reduction potential (-1.19 eV vs. SCE, pH = 7) and for all Bi doped NaTaO₃ samples, the flat band potential was sufficient for the hydrogen generation.

Copyright © 2011, Hydrogen Energy Publications, LLC. Published by Elsevier Ltd. All rights reserved.

1. Introduction

Solar hydrogen is considered as one of the most promising and sustainable ways to generate clean energy [1–4]. In order to commercialize the solar hydrogen production, 10–15% energy conversion efficiency is desired from the photocatalytic material system, under the solar radiation [5,6]. However, suitable material systems which meet this target efficiency under visible radiation are still lacking and efforts are needed to explore the photophysical properties of novel materials. In the past a few years, several materials systems such as SrTiO₃, NaTaO₃, TiO₂, ZnS etc. have been thoroughly studied for the photocatalytic hydrogen production [6–10]. Various strategies have been adapted to achieve and enhance

the visible light photocatalytic activity. Doping in wide band gap photocatalysts such as Fe or Cr-doped TiO₂ [11], V-doped TiO₂ [12], preparing composites such as ZnO–CdS core shell nanostructures [13], TiO₂/CdS nano-composites [14], Pt/Cr₂O₃/TiO₂ [15], utilizing surface plasmonic effects as in Ag loaded TiO₂ [16–18] have been recently reported to gain the visible light hydrogen evolution. Among these strategies, doping in highly efficient wide band gap photocatalysts, is one of the most successful approaches to develop new compounds. Of the various photocatalysts studied, NaTaO₃ has been identified as an excellent photocatalyst for the water splitting reaction under UV radiation [19–22]. NaTaO₃ has sufficiently negative conduction band edge potential vs. H₂/H₂O reduction level (as indicated by empirical calculations) and possesses

* Corresponding author. Tel.: +65 6790 4256; fax: +65 6790 9081.

E-mail addresses: kanh0002@ntu.edu.sg (P. Kanhere), zhengjw@ihpc.a-star.edu.sg (J.W. Zheng), aszchen@ntu.edu.sg (Z. Chen).
0360-3199/\$ – see front matter Copyright © 2011, Hydrogen Energy Publications, LLC. Published by Elsevier Ltd. All rights reserved.
doi:10.1016/j.ijhydene.2011.12.056

delocalized nature of photoexcited electrons which are highly beneficial for the photocatalytic hydrogen generation [20]. The photocatalytic activity of NaTaO₃ has been further enhanced by doping of ions such as La, Sr, Ca, and Ba [23,24]. Particularly, 2% La doped NaTaO₃ nanoparticles loaded with (0.2 wt. %) NiO have demonstrated superior photocatalytic behavior under 270 nm radiation [25]. In addition, La doped NaTaO₃ system, synthesized by sol-gel method has been further improved by RuO₂ loading to achieve stoichiometric water splitting reaction [26]. However, NaTaO₃ has a large band gap value (~4.0 eV) and thus the material systems like La doped NaTaO₃ are not useful in the solar spectrum. Nevertheless, due to its unique set of properties and high activity under UV radiation, NaTaO₃ is considered as a good host material to modify the electronic structure and to potentially achieve the visible light photocatalysis. Recent studies have shown that doping of elements like Bismuth [27,28], Nitrogen [29] and co-doping of elements like La–Co [30], La–Cr [31,32], and La–Ir [33] in NaTaO₃ is useful in inducing visible light absorption and subsequent photocatalytic activities. The photocatalytic hydrogen evolution by Bismuth doped NaTaO₃ powders prepared by hydrothermal method has been studied by Li et al [27]. Further, small concentration of Bi doping in NaTaO₃ and its photocatalytic activity has been reported by Wang et al. [34]. Although Li and co-workers [27] have shown that Bi doped NaTaO₃ solid solution is useful for photocatalytic hydrogen generation, a complete understanding of Bi doped NaTaO₃ system is needed for further development. Oxides of Bismuth have narrow band gaps on account of Bi 6s orbital and earlier studies show that doping of Bi³⁺ in wide band gap photocatalysts has produced visible light absorption [35–37]. Therefore, it is essential to study the effect of Bi³⁺ doping in NaTaO₃ on the photophysical properties and photocatalytic hydrogen evolution. Further, NaTaO₃ is an important photocatalyst and the measurement of flat band potentials (on SCE scale) of pristine and Bi doped NaTaO₃ is essential to contribute to the further understanding of this phase. In our earlier work, we showed that the optical properties of Bi doped NaTaO₃ can be significantly changed by changing the synthesis conditions [28]. Bismuth doped NaTaO₃ system shows significant absorption in the visible region and thus holds a promise to develop visible light sensitive photocatalysts with high activity. In this study, we report the visible light driven ($\lambda > 390$ nm) photocatalytic hydrogen evolution from Bismuth doped NaTaO₃ powders up to 7.5% Bi doping. It was found that the doping concentration, synthesis conditions, and the amount of platinum co-catalyst loading significantly affect the photocatalytic properties. Further, the flat band potential of the pristine and Bi doped powders was estimated using Mott–Schottky plots. It was shown that doped NaTaO₃ powders can be potentially useful photocatalysts under the visible radiation.

2. Experimental details

2.1. Synthesis of materials

Pristine and Bi doped NaTaO₃ powders were prepared by the conventional solid-state method. The starting materials,

Ta₂O₅ (Alfa Aesar 99%), Bi₂O₃ (Sigma Aldrich 99%) and Na₂CO₃ (Univar 99.8%) were mixed in an agate type mortar, pressed into pellets and fired at 1173 K for 10 h using a platinum crucible in a muffle furnace in ambient atmosphere. In all, Bi doped NaTaO₃ powders with increasing Bi content (2.5%, 5.0%, 7.5%, and 10%) were synthesized with three different molar ratios of the starting materials. The molar ratios of Ta:Na:Bi are summarized in Table 1. In short, Na rich, Na deficient, and near stoichiometric conditions were maintained by adjusting the amount of Na₂CO₃ and Ta₂O₅. The series of samples synthesized under Na rich, Na deficient and near stoichiometric conditions are referred to as S1, S2, and S3, respectively. The purpose of applying different Na/Ta ratio is to adjust the optical properties of the final products through Bi site occupancy [28]. However since Na₂O evaporates more easily during synthesis, a small amount of excessive Na₂CO₃ was added as compensation. For example in the S3 samples, 1–3% more Na was used in the starting reagents to achieve targeted equal occupancy of Bi in both Na and Ta sites. Platinum nanoparticles were loaded on the surface of doped NaTaO₃ by chemical impregnation method. Appropriate amount of catalyst powder and platinum precursor (H₂PtCl₆·6H₂O, Sigma–Aldrich) were mixed in the agate type mortar. The suspension was continuously stirred and heated at 75 °C till it dried. The powder was further heated at 300 °C for 1 h.

2.2. Characterization

The phase and crystal structure were studied by analysis of X-ray diffraction patterns. (Bruker D8 Advance; Cu K α = 1.54 Å). The XRD patterns were recorded within 2 θ range of 20°–100° with the steps of 0.03° and time of 1 s per step. The optical properties of the powders were studied by diffused reflectance spectroscopy (DRS) using ultraviolet–visible absorption spectrometer (Shimadzu 2051 PC). The band gap values of the samples were estimated by Kubelka–Munk analysis, assuming direct band gaps. The morphology of the samples was analyzed by scanning electron microscope (JOEL 6400F) and the quantitative chemical analysis was done by EDS attachment using standard-less ZAF method. The flat band potentials of the photocatalysts were estimated by Mott–Schottky plots (1/C² vs. V). The electrochemical cell contained the working electrode made up of photocatalyst coated on FTO (surface, area = 3.5 cm²), counter electrode (platinum plate, area = 1.5 cm²) and reference electrode (saturated calomel electrode). The electrochemical measurements were carried out in dilute NaOH electrolyte of pH 10.5. A small AC signal of 100 Hz was applied between the working and counter electrodes and modulated DC bias was

Table 1 – The ratios of initial reactants used to synthesize Bi doped NaTaO₃ samples.

	Ta	Na	Bi
Series 1(S1)	1–x	1	x
Series 2(S2)	1	1–x	x
Series 3(S3)	1	1.01–1.03	x

systematically varied from +0.2 to –1.2 V using Gamry 300G potentiostat. To prepare the working electrode, 150 mg of photocatalyst powder was suspended in 1 mL of ethanol and the slurry so formed was applied to FTO glass. The coated FTO glass was subsequently dried at 80 °C for 2 h. The surface area of the samples was estimated by BET technique. Adsorption isotherms were recorded at –196 °C after 6 h of degassing, using Micrometrics ASAP 2020 surface area analyzer.

2.3. Photocatalytic hydrogen evolution

The photocatalytic reaction was carried out in a closed-gas circulation system with a reaction cell made up of Pyrex glass and quartz window for vertical illumination. A 800 W high pressure Xe lamp (Oriole Instruments, USA) was used as a light source. A 390 nm cut off filter was employed to block the deep UV light. The average intensity at the surface of the solution was measured to be 150 mW/cm². The IR component in the radiation was removed by a filter containing circulating water. The reaction temperature was maintained at 25 °C with the help of an external water circulation jacket. All the reactions were carried out in argon gas atmosphere. In all tests, 50 mg of catalyst was suspended in 80 mL of deionized water and 20 mL of methanol by magnetic stirring. The reaction was carried out for 12 h and the amount of hydrogen evolved was analyzed at every 2 h by gas chromatograph (Shimadzu GC-2014; Molecular sieve 5 A, TCD detector, Ar carrier gas). It was confirmed that no hydrogen was evolved under dark conditions with or without catalyst.

3. Results and discussion

3.1. Crystal structure and microstructure

X-ray diffraction patterns of all the samples conformed to space group No. 62 (Pbnm) [38]. The representative XRD patterns of the pristine and 7.5% Bi doped samples in the series S1, S2, and S3 are shown in Fig. 1a–d. The samples in all the series showed presence of a monophasic up to 7.5% Bi doping. A small amount of impurity phase of Bi₂O₃ was detected for 10% Bi doping and thus the present study was limited to a maximum of 7.5% Bi doping. Fig. 2 shows the variation in the unit cell volumes of the samples in the series S1, S2, and S3. All the doped samples showed increment in the cell volumes along with Bi content and this increment was consistent with the ionic radii of Bi³⁺ (1.03 Å), Na¹⁺ (1.01 Å) and Ta⁵⁺ (0.64 Å) [39]. Impurity free XRD patterns and systematic increments in the unit cell volumes (Bi³⁺ > Ta⁵⁺), (Bi³⁺ > Na¹⁺) indicated that Bi was accommodated in the lattice, for all the doped samples. The expansion of the unit cell volume was largest for the samples in the series S2, while it was the minimum for the samples in the series S3. It is worth noting, that the initial stoichiometry of these samples was different. The samples in the series S1, were prepared under Na-rich conditions ($M_{\text{Na}} = M_{\text{Ta}} + M_{\text{Bi}}$), thus it is proposed that majority of Bi ions occupy Ta site. This prediction was consistent with the lack of Na₂O or NaBiO₂ impurities in the XRD pattern. Similarly, the samples in the series S2 were prepared under Na-deficient conditions ($M_{\text{Na}} + M_{\text{Bi}} = M_{\text{Ta}}$),

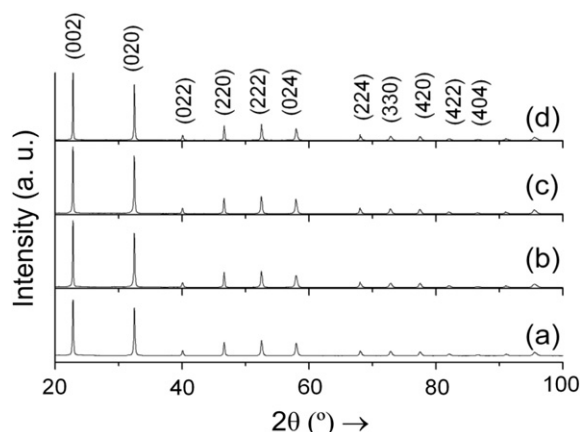


Fig. 1 – XRD patterns of (a) pristine NaTaO₃ and 7.5% Bi doped NaTaO₃ in the series (b) S1, (c) S2, and (d) S3.

and thus majority of Bi ions are expected to occupy Na site. In this case, the impurities such as Ta₂O₅ and oxide complexes of bismuth and tantalum were absent up to 7.5% doping. The samples from the series S3 were prepared under mildly Na-rich conditions. These conditions allowed Bi ions to occupy both Na and Ta sites in the lattice. The site occupancy values of Bi ion obtained from the Rietveld refinement results were consistent with the predicted stoichiometry (See supporting information). Thus it is proposed that Bi ions occupy different sites in the lattice under different synthesis conditions.

Fig. 3a–d show a comparison of the morphologies of the pristine and 7.5% Bi doped samples in the series S1, S2, and S3. The pristine NaTaO₃ powders showed cuboid shaped particles with a large particle size variation, ranging from 200 to 800 nm (Fig. 3-a). The particles in the series S1 were smaller in size as compared to that of the pristine NaTaO₃, ranging from 100 to 400 nm. These particles showed cuboid shapes with sharp edges (Fig. 3-b). On the other hand, the particles in the series S2 showed clear agglomeration. These particles were no longer cuboids but rather irregular in shape and larger in size as compared to that of the pristine NaTaO₃ (Fig. 3-c). The particles in the series S3 showed sharp edges and facets with reduced particles size as compared to that of the pristine NaTaO₃. Prominent rectangular shapes and sharp facets were

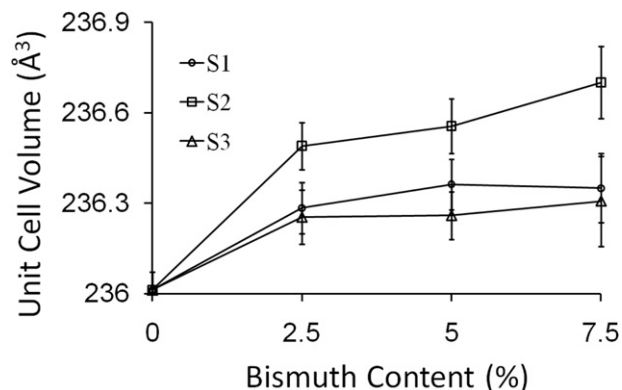


Fig. 2 – The variation in unit cell volumes of Bi doped NaTaO₃ powders in the series S1, S2, and S3.

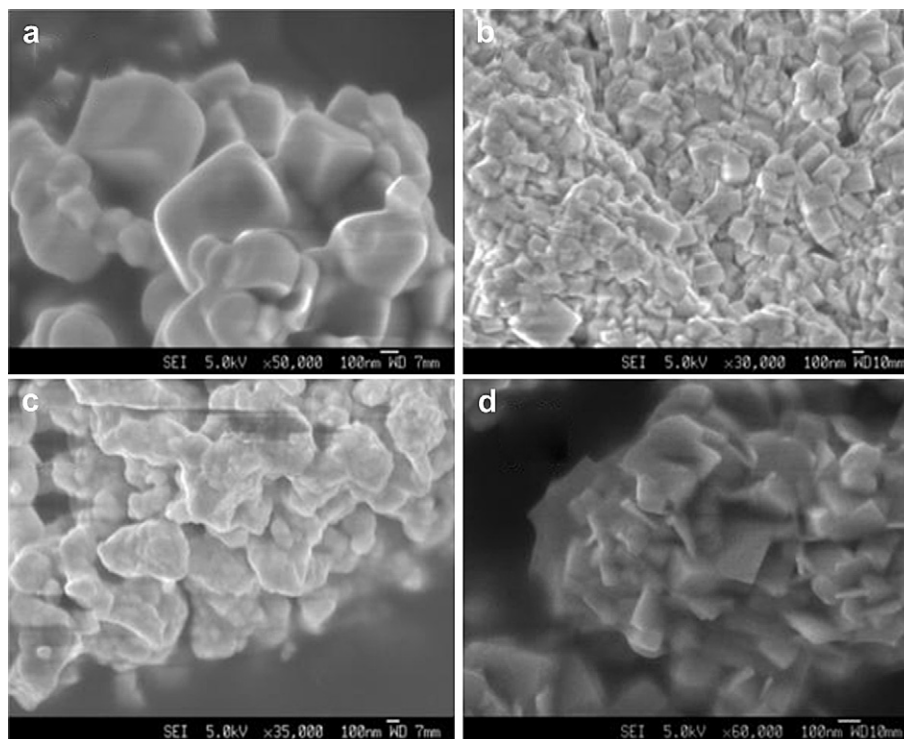


Fig. 3 – Field emission scanning electron microscope images of (a) pristine NaTaO_3 and 7.5% Bi doped NaTaO_3 in the series (b) S1, (c) S2, and (d) S3.

seen in the SEM observation of the particles in the series S3 (Fig. 3-d). The irregular and agglomerated growth of the samples in the series S2 indicated that the crystallinity of these powders was reduced. This result was consistent with the crystallite size values obtained from the XRD analysis (See supporting information). In the preparation of NaTaO_3 , excessive Na acts as a flux which promotes the grain growth, therefore under Na-deficient conditions the reduced crystallinity was observed [25]. Fig. 4 shows that bright field images of

bare and Pt loaded surfaces of 7.5% Bi doped NaTaO_3 (S3 series). The TEM images confirmed that uniform loading of platinum nanoparticles occurred on the catalysts surface. Although samples in S1, S2, and S3 series showed different particle shapes and sizes, the surface area of the samples estimated by B.E.T. method did not differ significantly. The surface area values of the pristine and Bi doped NaTaO_3 samples are listed in Table 2. It is noted that the surface area values are in the range of 1–2 m^2/g .

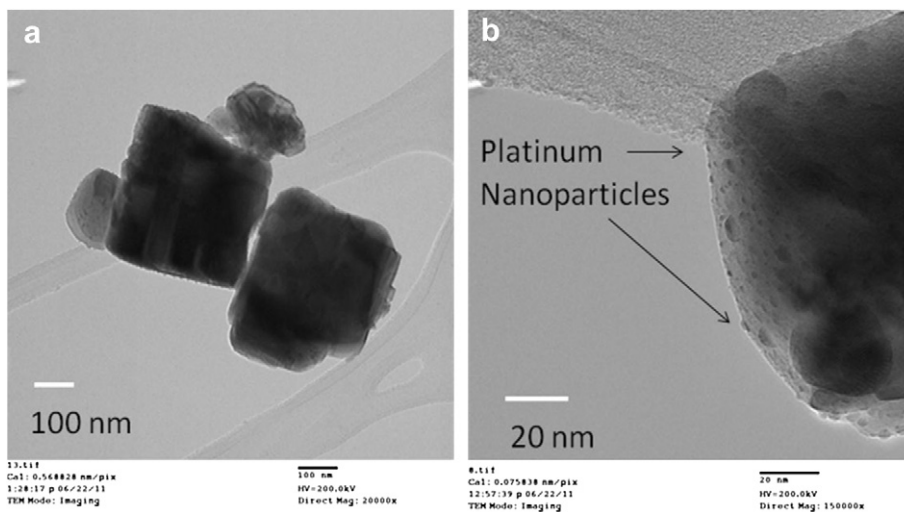


Fig. 4 – Transmission electron microscope images of (a) 7.5% Bi doped NaTaO_3 particles (b) 0.06% Pt loaded 7.5% Bi doped NaTaO_3 particles in the series S3.

Table 2 – The surface area values of the pristine and Bi doped NaTaO₃ powders estimated by BET method.

Bi doping concentraion/Surface area (m ² /g)	S1	S2	S3
0.0	1.13	1.13	1.13
2.5	0.95	1.05	1.11
5.0	1.15	1.02	1.12
7.5	1.46	1.34	1.22

3.2. Optical absorption spectra

The optical absorption spectra of the samples in the series S1, S2, and S3 are shown in Fig. 5a–c respectively. The band gap value of the pristine NaTaO₃ was found to be 4.01 eV. The absorption spectra of all of the doped samples showed extension towards longer wavelength along with the increase in Bi content, indicating that change in the optical absorption is caused by Bismuth doping. The band gap values of the samples, estimated by Kubelka–Munk function are presented in Table 3. It was observed that the absorption edge of S1 samples (Fig. 5a) was shifted towards the visible wavelengths. The band gap values were found to be in the

visible region, except for 2.5% Bi doping. The poor absorption of 2.5% Bi doped sample may be attributed to low dopant concentration. On the other hand, the samples in S2 series did not show visible light absorption ($\lambda > 400$ nm) (Fig. 5b). However, a small extension towards longer wavelengths was observed and the estimated band gap values were in the UV region. The samples in S3 showed intense visible light absorption extending up to 550 nm (Fig. 5c). The lowest band gap value of 2.64 eV was obtained for 7.5% Bi doping in this series. Similar to the S1 series, 2.5% Bi doped sample in S3 series showed poor absorption in the visible region. The band gap values of the samples in S3 series were significantly lower than that of the S1 and S2 samples. Further, it was seen that the band gap value reduced with increased content of Bi doping. The above results indicate that extent of the band gap narrowing is dependent on the Bismuth content in the lattice as well as initial stoichiometry of the starting materials (Na/Ta ratio). The chemical analysis (EDS and XPS) confirmed that the Bi³⁺ ions were present in all the samples irrespective of the synthesis conditions (See supporting information). Therefore, it was clear that the optical properties were function of the site occupancies of Bi ions at A and B site in the lattice.

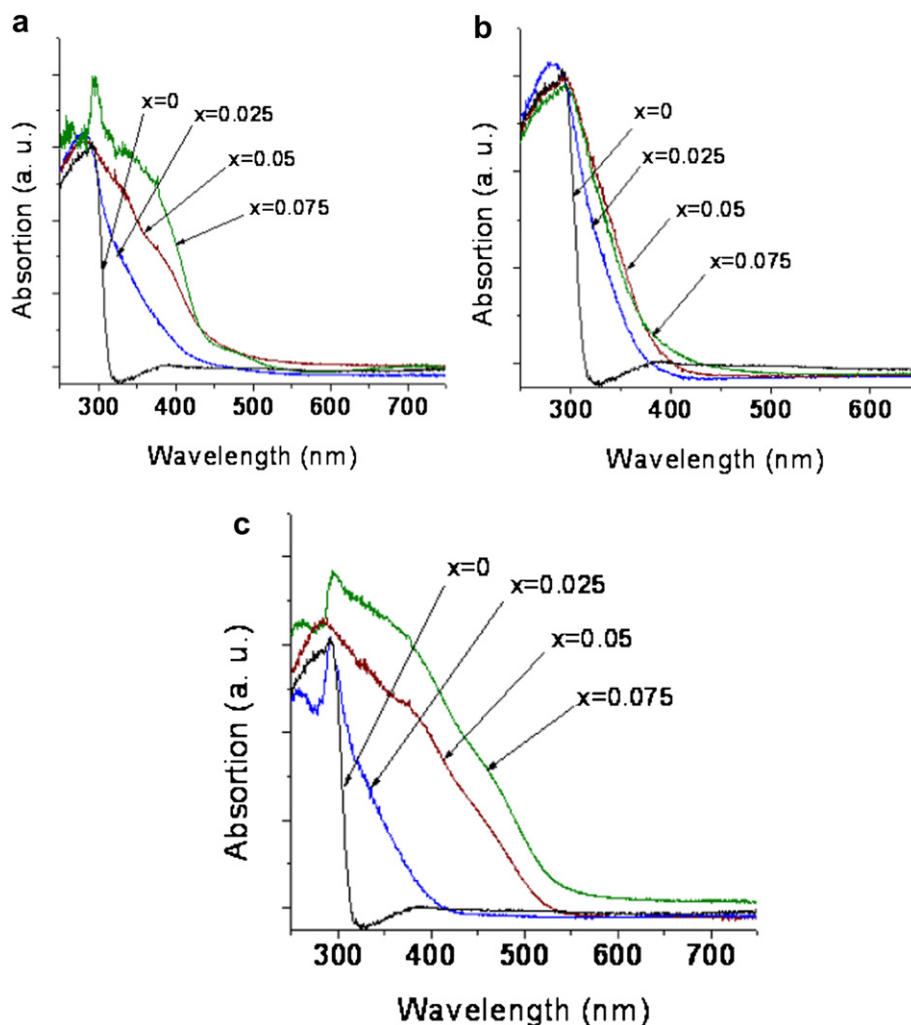


Fig. 5 – Diffused reflectance spectra of Bi doped NaTaO₃ samples in the series (a) S1, (b) S2, and (c) S3; x is the fractional bismuth content.

Table 3 – The band gap values of Bi doped NaTaO₃ samples obtained by Kubelka–Munk analysis.

Series/Bi content (%)	S1(eV)	S2(eV)	S3(eV)
0	4.01	4.01	4.01
2.5	3.65	3.75	3.85
5.0	3.05	3.65	2.77
7.5	2.95	3.65	2.64

3.3. Band diagrams

Fig. 6 shows the Mott–Schottky plots of the pristine and Bi doped NaTaO₃ powders at pH = 10.5. The linear part of $1/C^2$ vs. V curve was extrapolated to estimate the flat band potential of the photocatalyst. The flat band potential of the pristine NaTaO₃ was found to be -1.19 eV vs. SCE at pH = 7. The flat band potential of this phase is predicted to be -1.07 eV vs. NHE (at pH = 0; -1.23 eV vs. SCE at pH = 7) by using the empirical relation proposed by Scaife [40]. The present result shows that the empirically calculated value agrees reasonably well with the one by experimental measurement. These results confirm that the CB potential of NaTaO₃ is highly negative to H₂/H₂O reduction level, which is one of the reasons of its high photocatalytic activity. The flat band potential of Bi doped NaTaO₃ in the series S1 and S3 was found to be 0.25 eV and 0.08 eV more positive to that of the pristine NaTaO₃. On the other hand, the flat band potential of the sample in the series S2 shifted to more negative values by 0.15 eV. The present results show that all the doped samples have enough potential to evolve hydrogen. It is further noted that occupancy of the Bi ions at Ta site lowered the CB potential by a small amount as seen from S1 and S3 samples. In our earlier work, we showed that Bi substitution at different lattice sites in NaTaO₃ resulted in the appearance of mid-gap states in the band gap [28]. The substitution of Bi at Ta site created extra states in the band gap below the CB while substituting Bi at Na site did not change the band gap significantly. On the other hand, when Bi was substituted at both Na and Ta sites, the energy states appeared in between the band gap. DFT calculations showed

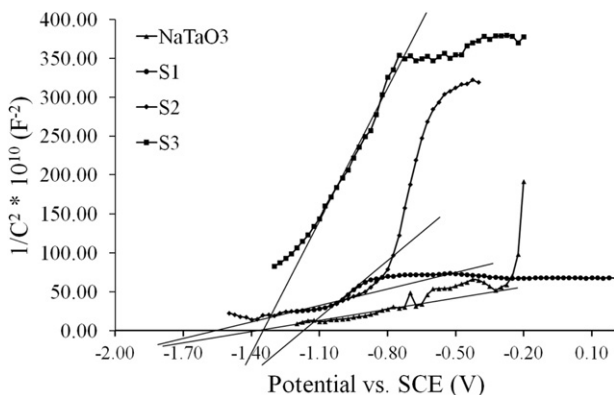


Fig. 6 – Mott–Schottky plots of the pristine NaTaO₃ and 7.5% Bi doped NaTaO₃ powders in the series S1, S2, and S3 recorded at 100 Hz, at pH = 10.5 (vs SCE electrode). The flat band potential of NaTaO₃ = -1.40 eV; S1 = -1.15 ; S2 = -1.55 eV; S3 = -1.32 eV vs. SCE at pH = 10.5.

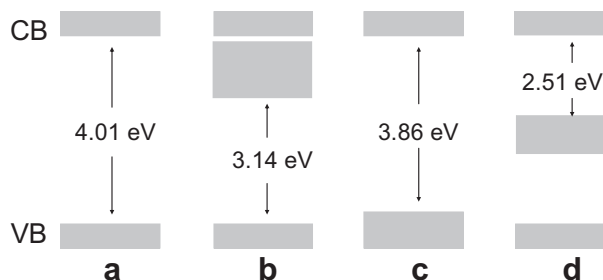


Fig. 7 – The band gap narrowing mechanism of (a) pure and (b) NaTa_{1-x}Bi_xO₃, (c) Na_{1-x}Bi_xTaO₃ and (d) Na_{1-x}Bi_xTa_{1-x}Bi_xO₃ (x = 0.0625).

that the band gap values of Bi doped NaTaO₃ system decrease in by 0.15 eV for Bi at Na site, 1.5 eV for Bi at both Na and site, 0.87 eV for Bi at Ta site. Upon substitution of Bi at Ta site, the effective CB potential shifted to more positive values (Fig. 7). On the contrary, substitution of Bi at Na site left the CB potential unchanged and the effective VB is shifted towards negative potentials. Interestingly, for the substitution of Bi at both Na and Ta sites, Bi 6s induced filled energy states appeared in between the band gap and thus the effective VB potential shifted towards lower energy values. The measured flat band potentials show a similar trend as indicated by the DOS analysis; however discrepancy exists between the two sets of the data.

3.4. Photocatalytic hydrogen evolution

Bi doped NaTaO₃ samples did not show significant hydrogen evolution without loading of platinum co-catalyst under the visible light irradiation. Fig. 8 shows the effect of varying amount of platinum loading on the photocatalytic hydrogen evolution from 7.5% Bi doped sample in the S3 series. This series was selected to optimize the platinum loading as it showed the maximum visible light absorption. The hydrogen yield was the maximum for 0.06% loading of platinum. It was observed that for the same amount of platinum loading, the samples in the series S1 and S2 did not show hydrogen

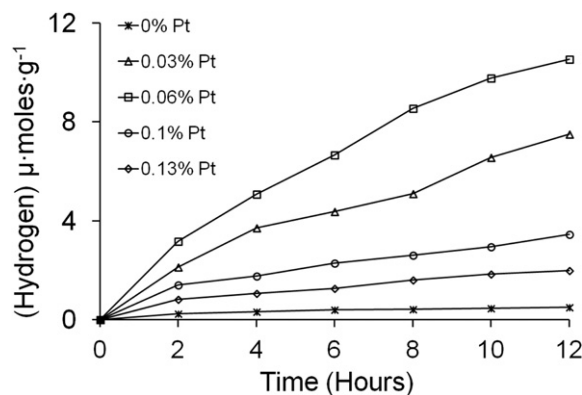


Fig. 8 – The effect of Platinum loading on the photocatalytic hydrogen evolution from 7.5% Bi doped NaTaO₃ samples in the series S3 (20 mL CH₃OH, 80 mL D.I. water; $\lambda > 390$ nm).

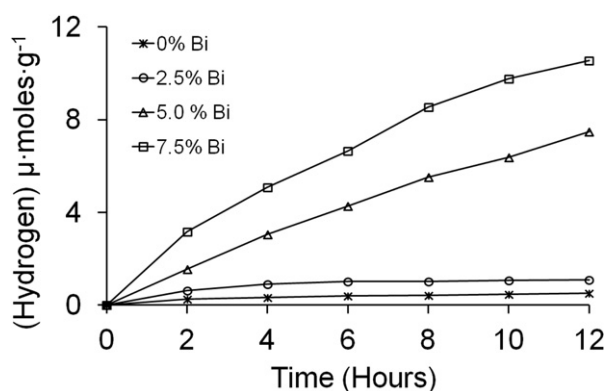


Fig. 9 – The photocatalytic hydrogen evolution from 0.06% Pt loaded samples in the series S3 with increasing Bi content (20 mL CH₃OH, 80 mL D.I. water; $\lambda > 390$ nm).

evolution. The samples in the series S3 showed increasing rates of hydrogen evolution along with Bi content (Fig. 9). However, 2.5% Bi doping showed no measurable H₂ evolution. Thus maximum rate of hydrogen evolution (0.86 $\mu\text{mol h}^{-1} \text{g}^{-1}$) was obtained for 7.5% Bi doped sample in the series S3 (near stoichiometric conditions). Although the present yield of hydrogen is still low as compared to the other reports, these results shed light on Bi³⁺ doping in NaTaO₃ system and its photocatalytic activities. In contrast to the reported work on Bi⁵⁺ doping [27], this work explains the hydrogen evolution characteristics of Bi doped NaTaO₃ compounds with Bi doping at different sites. Although all the samples showed enough CB overpotential, their optical properties and crystal structures differed significantly. The samples in the series S3 showed intense visible light absorption and thus the estimated band gap values were lower than those of the samples in S1 and S2 series. It was proposed that the S3 samples contained Bi ions at both Na and Ta sites in the lattice in approximately equal proportion. The occupancy of Bi ions at both Na and Ta sites helps maintain the ionic charge balance and thus minimize the native defects produced. On the other hand, the occupancy of Bi ions at Ta site would result in the generation of oxygen vacancy related defects while the occupancy of Bi ions at Na site would result in the cation vacancy related defects. These defects may act as electron-hole recombination centers and reduce the photocatalytic activity. Therefore the electronic structure and the crystal structure of samples in the series S3 were favorable for the photocatalytic hydrogen evolution.

4. Conclusions

The present work investigates photophysical properties and photocatalytic hydrogen generation of Bi doped NaTaO₃ powders up to 7.5% Bi doping. The main conclusions of the study are summarized as follows.

- By employing the appropriate synthesis conditions (Na/Ta ratio close to unity), the band gap values of Bi doped NaTaO₃ powders can be narrowed to as low as 2.64 eV for 7.5% Bi

doping. However, low molar concentrations ($\sim 2.5\%$) of Bi are not useful to induce the visible light absorption. It was found that the synthesis condition (starting Na/Ta ratio) affects the band gap narrowing and the point defects in the doped photocatalysts, resulting in the differences in the hydrogen yield.

- The CB potential of the pristine NaTaO₃ is highly negative to H₂/H₂O reduction level (-1.19 eV vs. SCE at pH = 7) and Bi doped NaTaO₃ powders show variations in the flat band potential according to the doping site. In general, both doped and undoped samples have sufficient overpotential for hydrogen generation. However the visible light activity depends on the Bi site occupancy.
- With the optimum loading of platinum nanoparticles, photocatalytic hydrogen evolution (0.86 $\mu\text{mol h}^{-1} \text{g}^{-1}$) occurs from 7.5% Bi doped NaTaO₃. Bi doped NaTaO₃ powders have demonstrated attractive photophysical properties providing a foundation for a further development of visible light active photocatalysts for hydrogen generation.

Acknowledgments

Financial support from MOE Singapore (Grant RG 112/05) is gratefully acknowledged. We are grateful to Dr. Martin K. Schreyer in ICES for the numerous technical discussions on crystal structures.

Appendix. Supplementary data

Supplementary data associated with this article can be found, in the online version, at [doi:10.1016/j.ijhydene.2011.12.056](https://doi.org/10.1016/j.ijhydene.2011.12.056).

REFERENCES

- [1] Nowotny J, Sorrell CC, Sheppard LR, Bak T. Solar-hydrogen: environmentally safe fuel for the future. *International Journal of Hydrogen Energy* 2005;30(5):521–44.
- [2] Bak TN J, Rekas M, Sorrell CC. Photo-electrochemical hydrogen generation from water using solar energy. materials-related aspects. *International Journal of Hydrogen Energy* 2002;27(10):991–1022.
- [3] Jing D, Guo L, Zhao L, Zhang X, Liu H, Li M, et al. Efficient solar hydrogen production by photocatalytic water splitting: from fundamental study to pilot demonstration. *International Journal of Hydrogen Energy* 2010;35(13):7087–97.
- [4] Dincer I. Green methods for hydrogen production. *International Journal of Hydrogen Energy*.
- [5] Kudo A, Miseki Y. Heterogeneous photocatalyst materials for water splitting. *Chemical Society Reviews* 2009;38(1):253–78.
- [6] Osterloh FE. Inorganic materials as catalysts for photochemical splitting of water. *Chemistry of Materials* 2008;20(1):35–54.

- [7] Puangpetch T, Sreethawong T, Chavadej S. Hydrogen production over metal-loaded mesoporous-assembled SrTiO₃ nanocrystal photocatalysts: effects of metal type and loading. *International Journal of Hydrogen Energy* 2010; 35(13):6531–40.
- [8] Kitano M, Hara M. Heterogeneous photocatalytic cleavage of water. *Journal of Materials Chemistry* 2010;20(4):627–41.
- [9] Wang L, Wang W, Shang M, Yin W, Sun S, Zhang L. Enhanced photocatalytic hydrogen evolution under visible light over Cd_{1-x}Zn_xS solid solution with cubic zinc blend phase. *International Journal of Hydrogen Energy* 2010;35(1): 19–25.
- [10] Zhang Z, Hossain MF, Takahashi T. Photoelectrochemical water splitting on highly smooth and ordered TiO₂ nanotube arrays for hydrogen generation. *International Journal of Hydrogen Energy* 2010;35(16):8528–35.
- [11] Dholam R, Patel N, Adami M, Miotello A. Hydrogen production by photocatalytic water-splitting using Cr- or Fe-doped TiO₂ composite thin films photocatalyst. *International Journal of Hydrogen Energy* 2009;34(13):5337–46.
- [12] Dholam R, Patel N, Miotello A. Efficient H₂ production by water-splitting using indium-tin-oxide/V-doped TiO₂ multilayer thin film photocatalyst. *International Journal of Hydrogen Energy* 2011;36(11):6519–28.
- [13] Wang X, Liu G, Lu GQ, Cheng HM. Stable photocatalytic hydrogen evolution from water over ZnO–CdS core-shell nanorods. *International Journal of Hydrogen Energy* 2010; 35(15):8199–205.
- [14] Liu Y, Zhou H, Zhou B, Li J, Chen H, Wang J, et al. Highly stable CdS-modified short TiO₂ nanotube array electrode for efficient visible-light hydrogen generation. *International Journal of Hydrogen Energy* 2011;36(1):167–74.
- [15] Yao W, Huang C, Muradov N, T-Raissi A. A novel Pd-Cr₂O₃/CdS photocatalyst for solar hydrogen production using a regenerable sacrificial donor. *International Journal of Hydrogen Energy* 2011;36(8):4710–5.
- [16] Chuang HY, Chen DH. Fabrication and photoelectrochemical study of Ag@TiO₂ nanoparticle thin film electrode. *International Journal of Hydrogen Energy* 2011;36(16): 9487–95.
- [17] Alenzi N, Liao WS, Cremer PS, Sanchez-Torres V, Wood TK, Ehlig-Economides C, et al. Photoelectrochemical hydrogen production from water/methanol decomposition using Ag/TiO₂ nanocomposite thin films. *International Journal of Hydrogen Energy* 2010;35(21): 11768–75.
- [18] Simon Q, Barreca D, Bekermann D, Gasparotto A, MacCato C, Comini E, et al. Plasma-assisted synthesis of Ag/ZnO nanocomposites: first example of photo-induced H₂ production and sensing. *International Journal of Hydrogen Energy* 2011;36(24):15527–37.
- [19] Hu CC, Tsai CC, Teng H. Structure characterization and tuning of perovskite-like NaTaO₃ for applications in photoluminescence and photocatalysis. *Journal of the American Ceramic Society* 2009;92(2):460–6.
- [20] Kato H, Kudo A. Water splitting into H₂ and O₂ on alkali tantalate photocatalysts ATaO₃ (A = Li, Na, and K). *Journal of Physical Chemistry B* 2001;105(19):4285–92.
- [21] Lee YW, Takata T, Hara T, Yoshimura M, Domen K. Hydrothermal synthesis of fine NaTaO₃ powder as a highly efficient photocatalyst for overall water splitting. *Bulletin of the Chemical Society of Japan* 2007;80(2):423–8.
- [22] Lin WH, Cheng C, Hu CC, Teng H. NaTaO₃ photocatalysts of different crystalline structures for water splitting into H₂ and O₂. *Applied Physics Letters* 2006;89(21). Article No. 211904.
- [23] Kudo A, Kato H. Effect of lanthanide-doping into NaTaO₃ photocatalysts for efficient water splitting. *Chemical Physics Letters* 2000;331(5–6):373–7.
- [24] Torres-Martínez LM, Cruz-Lopez A, Juárez-Ramírez I, Meza-de LR, Ma E. Methylene blue degradation by NaTaO₃ sol-gel doped with Sm and La. *Journal of Hazardous Materials* 2009;165(1–3):774–9.
- [25] Kato H, Asakura K, Kudo A. Highly efficient water splitting into H₂ and O₂ over lanthanum-doped NaTaO₃ photocatalysts with high crystallinity and surface nanostructure. *Journal of the American Chemical Society* 2003;125(10):3082–9.
- [26] Torres-Martínez LM, Gómez R, Vázquez-Cuchillo O, Juárez-Ramírez I, Cruz-López A, Alejandre-Sandoval FJ. Enhanced photocatalytic water splitting hydrogen production on RuO₂/La:NaTaO₃ prepared by sol-gel method. *Catalysis Communications* 2010;12(4):268–72.
- [27] Li ZG, Wang YX, Liu JW, Chen G, Li YX, Zhou C. Photocatalytic hydrogen production from aqueous methanol solutions under visible light over Na(Bi_xTa_{1-x})O₃ solid-solution. *International Journal of Hydrogen Energy* 2009;34(1):147–52.
- [28] Kanhere PD, Zheng JW, Chen Z. Site Specific optical and photocatalytic properties of Bi-doped NaTaO₃. *Journal of Physical Chemistry C* 2011;115(23):11846–53.
- [29] Liu DR, Wei CD, Xue B, Zhang XG, Jiang YS. Synthesis and photocatalytic activity of N-doped NaTaO₃ compounds calcined at low temperature. *Journal of Hazardous Materials* 2010;182(1–3):50–4.
- [30] Yi ZG, Ye JH. Band gap tuning of Na_{1-x}La_xTa_{1-x}Co_xO₃ solid solutions for visible light photocatalysis. *Applied Physics Letters* 2007;91(25). Article No. 254108.
- [31] Yang M, Huang X, Yan S, Li Z, Yu T, Zou Z. Improved hydrogen evolution activities under visible light irradiation over NaTaO₃ codoped with lanthanum and chromium. *Materials Chemistry and Physics* 2010;121(3):506–10.
- [32] Yi ZG, Ye JH. Band gap tuning of Na_{1-x}La_xTa_{1-x}Cr_xO₃ for H₂ generation from water under visible light irradiation. *Journal of Applied Physics* 2009;106(7). Article No. 074910.
- [33] Iwase A, Saito K, Kudo A. Sensitization of NaMO₃ (M: Nb and Ta) photocatalysts with wide band gaps to visible light by Ir doping. *Bulletin of the Chemical Society of Japan* 2009;82(4): 514–8.
- [34] Wang XJ, Bai HL, Meng Y, Zhao YJ, Tang CH, Gao H. Synthesis and optical properties of Bi³⁺ doped NaTaO₃ nano-size photocatalysts. *Journal of Nanoscience and Nanotechnology* 2010;10:1788–93.
- [35] Wu Y, Lu G, Li S. The doping effect of Bi on TiO₂ for photocatalytic hydrogen generation and photodecolorization of rhodamine B. *Journal of Physical Chemistry C* 2009;113(22): 9950–5.
- [36] Rengaraj S, Li XZ. Enhanced photocatalytic reduction reaction over Bi³⁺-TiO₂ nanoparticles in presence of formic acid as a hole scavenger. *Chemosphere* 2007;66(5):930–8.
- [37] Xu XH, Wang M, Hou Y, Yao WF, Wang D, Wang H. Preparation and characterization of Bi-doped TiO₂ photocatalyst. *Journal of Materials Science Letters* 2002; 21(21):1655–6.
- [38] Ahtee M, Darlington CNW. Structures of NaTaO₃ by Neutron powder diffraction. *Acta Crystallographica B* 1980;36: 1007–14.
- [39] Shannon RD. Revised effective ionic radii and systematic studies of interatomic distances in halides and chalcogenides. *Acta Crystallographica* 1976;32:751. Sect. A.
- [40] Scaife DE. Oxide semiconductors in photoelectrochemical conversion of solar energy. *Solar Energy* 1980;25(1):41–54.